Journal of
Climate Change Research
2020, 1(4): 89-109
DOI: 10.30488/CCR.2020.255527.1030

Climatic changes and astrochronology: an Ordovician perspective

Mansoureh Ghobadi Pour[1,2], Leonid Popov[2], Lesley Cherns[3]

[1] Department of Geology, Faculty of Sciences, Golestan University, Gorgan 49138-15739, Iran
[2] Department of Natural Sciences, National Museum of Wales, Cardiff, CF10 3NP, United Kingdom
[3] School of Earth and Environmental Sciences, Cardiff University, Cardiff, CF10 3AT, United Kingdom

Keywords
Ordovician
Orbital forcing
Astrochronology
Cyclostratigraphy
Biostratigraphy

Corresponding author
Mansoureh Ghobadi Pour
mghobadipour@yahoo.co.uk
m.ghobadipour@gu.ac.ir

Article history
Received: August, 27
Revised: October, 23
Accepted: November, 22

Abstract

Review of current progress in Mid to Late Ordovician astrochronological studies exposes some important issues related to cyclostratigraphical studies, including the completeness and correlation of successions, and the connection between inferred astronomical cycles and geological events recorded in the sedimentary record. While bulk, low-field, mass specific magnetic susceptibility methods are widely applied in studies of high resolution cyclostratigraphy, they require close support from sequence stratigraphy and biostratigraphy, and should be linked back to outcrop patterns. Otherwise they risk distortion in the calibration against geological time, through lack of anchoring to well-defined biostratigraphical horizons and unrecognised condensed intervals and larger hiatuses. A significant limitation currently is that few high-resolution radio-isotope ages are linked to well-defined biostratigraphical boundaries. Nevertheless, fourth order sedimentary sequences linked to 405 ky orbital eccentricity cycles, and longer orbital cyclicity impressed in third-order sequences, represent good grounds for development of a reliable astrochronological scale. The astrochronologically calibrated sequence-stratigraphical record documented from high latitude Gondwana shows significant impact from orbital forcing on the Mid to Late Ordovician global climate.

Introduction

For a long time the Ordovician was considered as a period of stable greenhouse climate (e.g. Gibbs et al. 2000; Church and Coe 2003) interrupted at the end by the short, but strong terminal (Hirnantian) Ordovician glaciation of the Southern Hemisphere which correlated with a major mass extinction event. This concept underwent substantial revision when it was convincingly demonstrated that intervals of relatively warm climate were interrupted periodically by short excursions of a significantly cooler climate coincident with global regressions, unstable sea level, significant shifts of climatic belts and complex biogeographical patterns (e.g. Saltzman and Young 2005; Page et al. 2007, Cherns and Wheeley 2007; Calner et al. 2010; Keller and Lehnart 2010; Loi et al. 2010). Quasi-periodic climatic changes recognised in the Ordovician can be linked to long-period orbital cycles (Turner et al. 2012; Cherns et al. 2013; Zhong et al. 2018; Fang et al. 2019). According to Laskar et al. (2004) this cycle remained relatively stable over c. 250 Ma and therefore it is considered as the most appropriate for astronomical calibration of Mesozoic and older time periods (Hinnov and Hilgen 2012). Major attention has focused on the analysis of modulation of the *g2–g5* 405 ky orbital eccentricity cycles with an estimated uncertainty of c. 500 ky over 250 Ma. They are expressed in the sedimentary record as fourth-order, high frequency sequences (Matthews and Frohlich 2002; Loi et al. 2010; Matthews and Al-Husseini 2010; Turner et al. 2012), and also can be extracted from the rock using magnetic susceptibility and gamma ray spectrometry (e.g. Elrich et al. 2013; Zhong et al. 2018; Fang et al. 2019).

Reliable anchoring of a floating Ordovician astrochronological time scale is hampered by shortage of high-resolution radio-isotope ages linked to distinct biostratigraphical boundaries. The ages inferred for the series and stage boundaries (Ogg et al. 2016; Figures 1, 2a) are mostly estimates with a

Please cite this article as Ghobadi Pour M, Popov L, Cherns L (2020) Climatic changes and astrochronology: an Ordovician perspective. Journal of Climate Change Research. 1(4): 89-109.

high level of uncertainty. For example, the $^{206}Pb/^{238}U$ age of 465.46 ± 3.53 Ma obtained by Mitchell et al. (1998) for a rich mid-Darriwilian graptolite fauna from the Argentinian Precordillera, considered biostratigraphically the best-constrained for the entire Ordovician by Cooper and Sadler (2012), has too high an uncertainty for reliable estimates of the age of the lower Darriwilian boundary and duration of the stage. Recently, the accuracy of estimates improved considerably for the Upper Ordovician, when the radio-isotope ages obtained by Ling et al. (2019) suggested 443.14 ± 0.24 Ma and 442.67 ± 0.24 Ma for the Hirnantian Stage base and top respectively, an estimated Hirnantian duration of only 0.47 ± 0.34 Ma, considerably shorter than previously expected (1.4 ± 2.05 Ma in the International Chronostratigraphic Chart ver. 2019/05; Ogg et al. 2016).

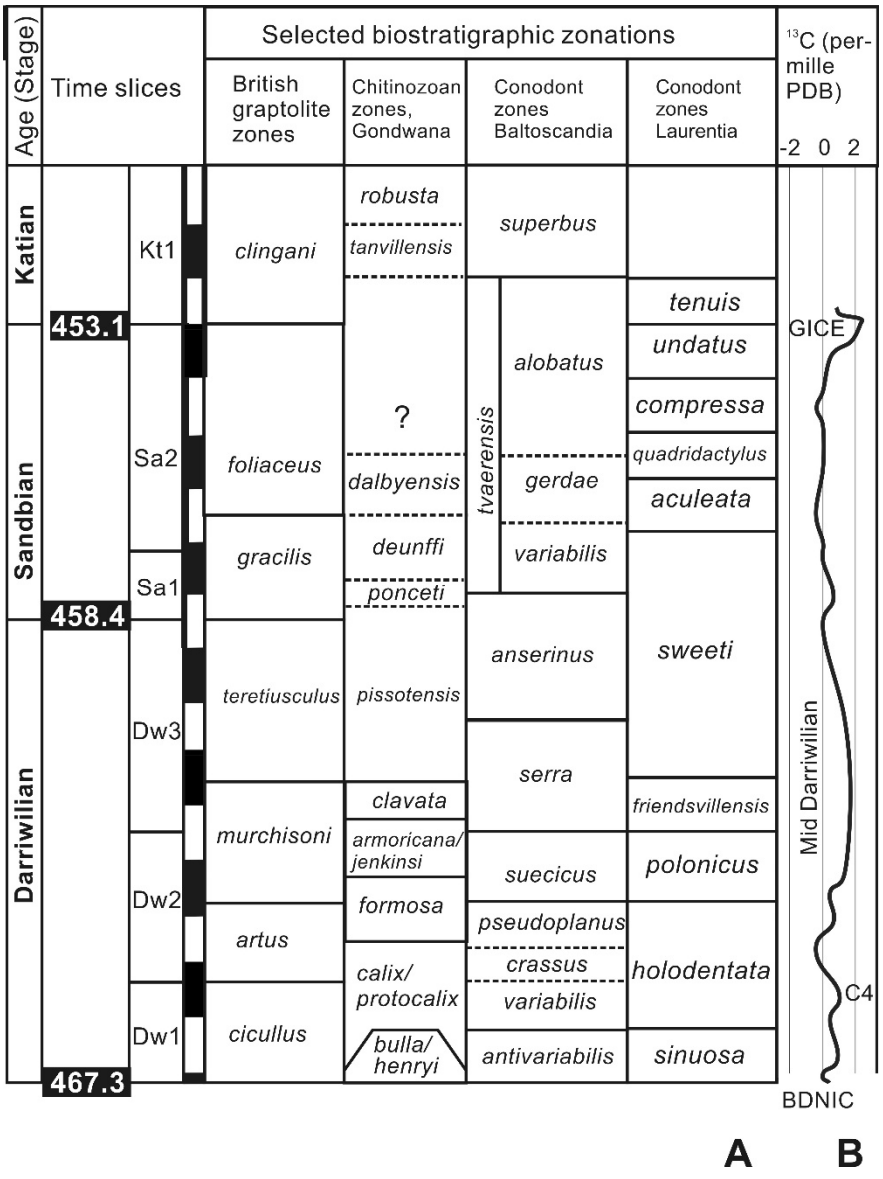

Figure 1. A, Correlation chart showing selected Darriwilian to early Katian biostratigraphical zonations and inferred epoch ages; **B,** $\delta^{13}C$ curve with major widespread stable isotope events (GICE, Guttenberg positive ICE; BDNICE, Basal Darriwilian negative ICE) mainly after Ogg et al. (2016);

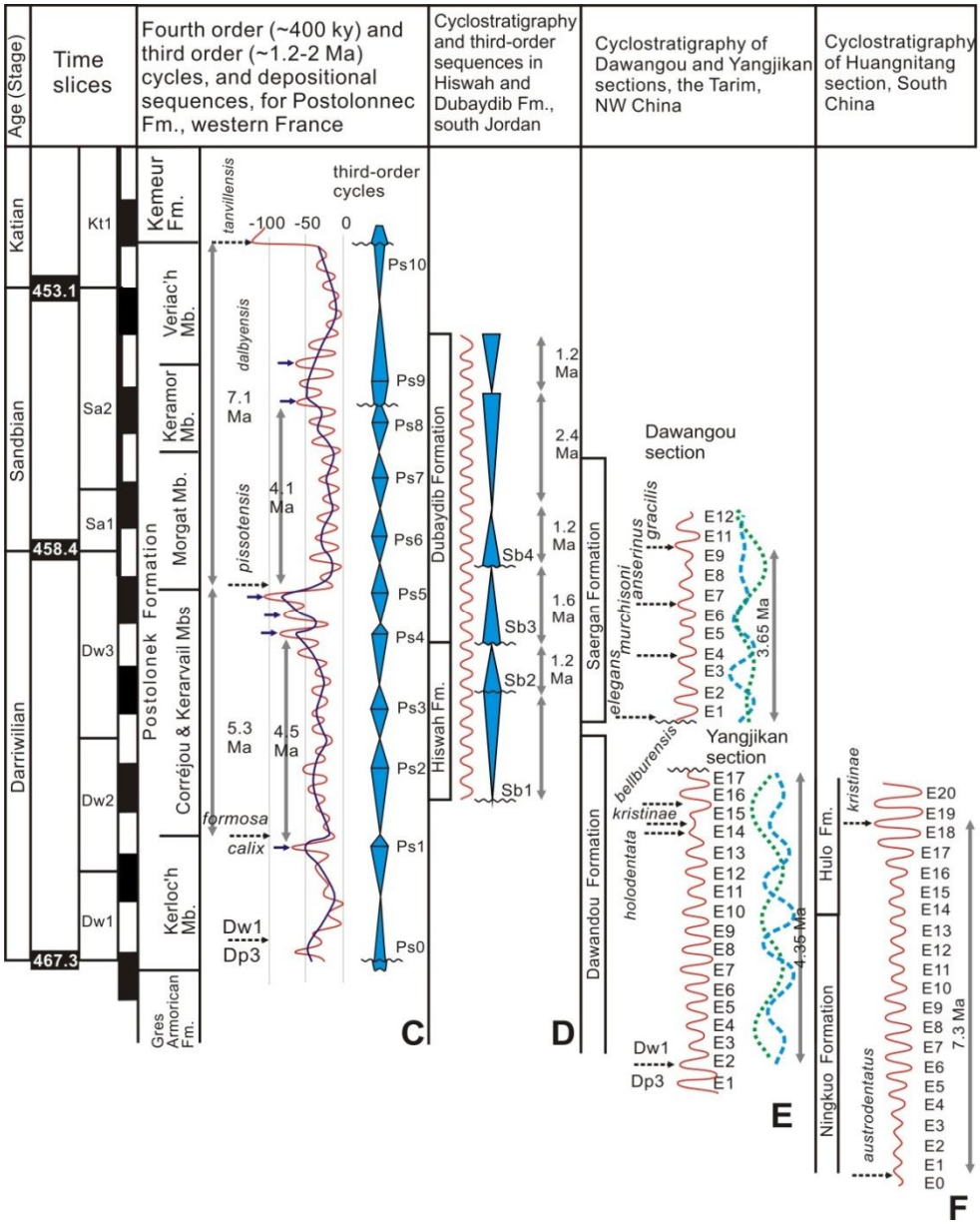

Figure 1 (continued). C, fourth order (~405 ky red line) and third order (~1.2-2 Ma dark blue line) cycles, and depositional sequences (with major disconformities), for the Postolonnec Formation of the Armorican Massif, western France showing inferred position of the lower Darriwilian boundary and FAD of selected biostratigraphically indicative chitinozoan taxa (after Dabard et al. 2015), high amplitude sea-level fluctuation pointed by arrows; **D,** fourth order sedimentary cycles (~405 ky red line) and six third order transgressive and aggradational to progradational sequences in Hiswah and Dubaydib formations, at southern Jordan, mainly after Turner et al. (2012); **E,** cyclostratigraphy of Dawangou and Yangjikan sections, the Tarim, NW China showing inferred 405 ky (red line), 1.2 Ma (blue line) and 2.4 Ma (green line) sedimentary cycles inferred position of the lower Darriwilian boundary and FAD of selected biostratigraphically indicative graptolite and conodont taxa (after Fang et al. 2019); **F,** cyclostratigraphy of Huangnitang section showing inferred 405 ky orbital eccentricity cycles (red line) and FAD of selected biostratigraphically indicative graptolite and conodont taxa (after Zhang et al. 2018). Inferred numerical ages of the stage boundaries shown in Ma.

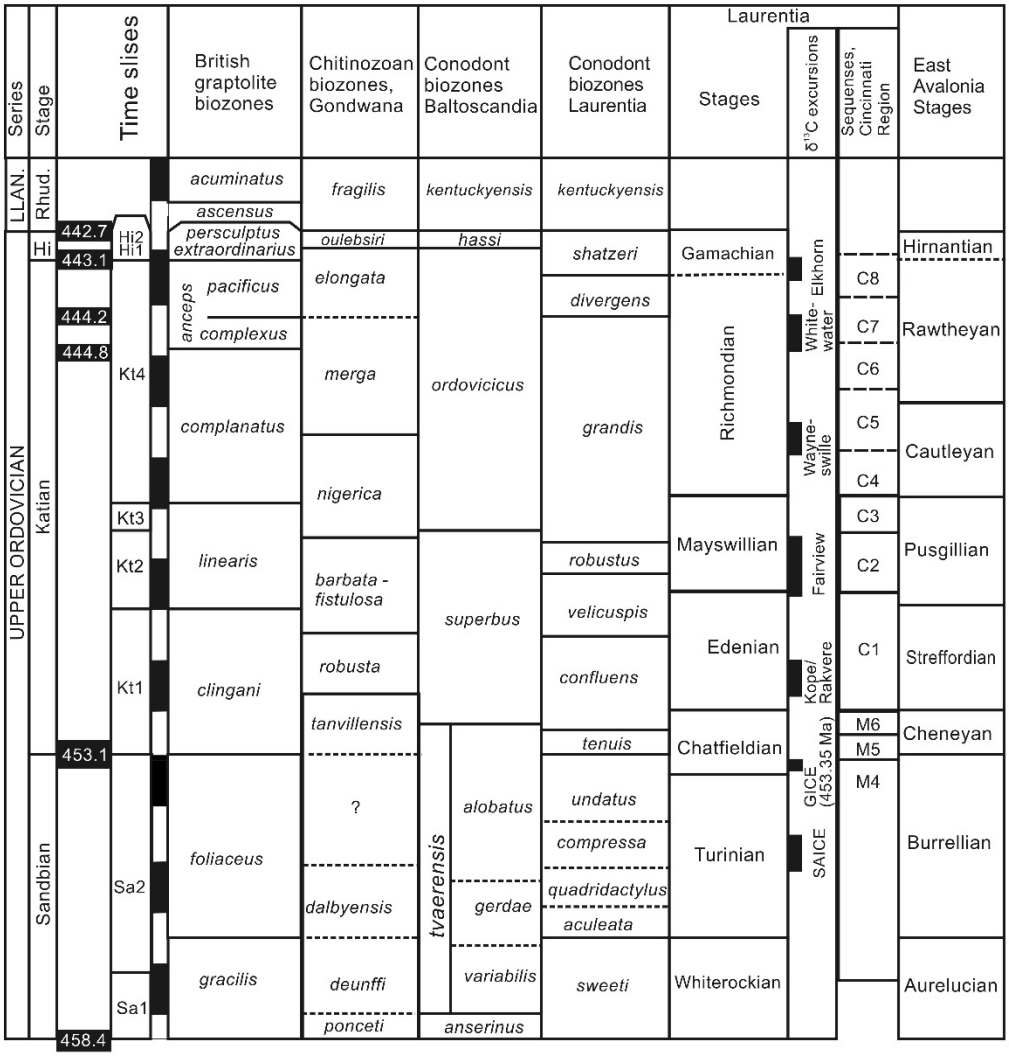

Figure 2. Correlation chart showing Sandbian to Hirnantian selected biostratigraphical zonations and inferred epoch ages, emended after Cooper and Sadler (2012), correlation of the upper Ordovician successions of Laurentia, Baltica, East Avalonia, Morocco, Siberia and South China, base of the depositional sequences for Cincinnati Region and $\delta^{13}C$ negative isotope excursions, after Bergstrom et al. (2010).

Metzger et al. (2020) used radio-isotope ages to constrain the duration of the GICE isotope event to less than 400 ky while the base of the Katian Stage was estimated as 453.12 ± 0.38 Ma. Thus, at present, high resolution radio-isotope ages for the top of the Ordovician System, the base of the Hirnantian and Katian stages are the best options for rooting floating astrochronological time scales.

A steadily increasing number of publications through the past decades have linked observed patterns of sedimentary cyclicity with inferred long-term astronomical cycles, carbon isotope excursions and major cooling episodes, mostly focused on the Mid and Late Ordovician. These publications represent an important step in building an integrated astronomically calibrated Ordovician time scale. However, they also expose some important issues related to the reliable rooting against biostratigraphical and geochronological markers that need to be properly addressed and discussed, notably the completeness of observed individual stratigraphical successions and their correlation, and the connection between inferred astronomical cycles and geological events recorded in the sedimentary record.

Records of modulation of 405 ky orbital eccentricity cycles in the Ordovician Mediterranean Gondwana

The most extensive Ordovician cyclostratigraphical record currently relates to Mediterranean Gondwana including North Africa and western Brittany (Loi et al. 2010; Videt et al. 2010; Dabard et al. 2015). Sophisticated methods were used to discriminate the amplitude and hierarchy of high-frequency

sedimentary cycles, including corrections for compaction, sediment load and tectonic subsidence. The fourth order genetic sequences, well expressed in the succession, were linked to 405 ky orbital eccentricity cycles and therefore can provide age/time estimates as discussed below. Both regions were parts of the Gondwana margin through the Ordovician Period (Figure 3) and located within high southern latitudes, probably 65°S and higher (Torsvik and Cocks 2011), thus short term climate fluctuations impacted strongly on sedimentation and its characteristics preserved in the sedimentary record. There is also relatively good biostratigraphical control mainly based on the Ordovician chitinozoan biozonation developed for high to temperate latitude Gondwana (Paris 1990; Figure 2a). The resulting eustatic sea-level curve (Figure 2b) is probably the most reliable and precise, and can be compared with a 'global' sea level curve produced by Haq and Schutter (2008) and Nielsen's (2004) Ordovician sea-level curve for Baltoscandia (Figure 2b). A significant problem for the Darriwilian to Hirnantian succession of Mediterranean Gondwana is accurate discrimination of stage boundaries based on First Appearance Datum (FAD) of graptolite species, when those graptolites are unknown in that part of Gondwana and precise correlation of boundaries in relation to the chitinozoan biozonation is not always possible.

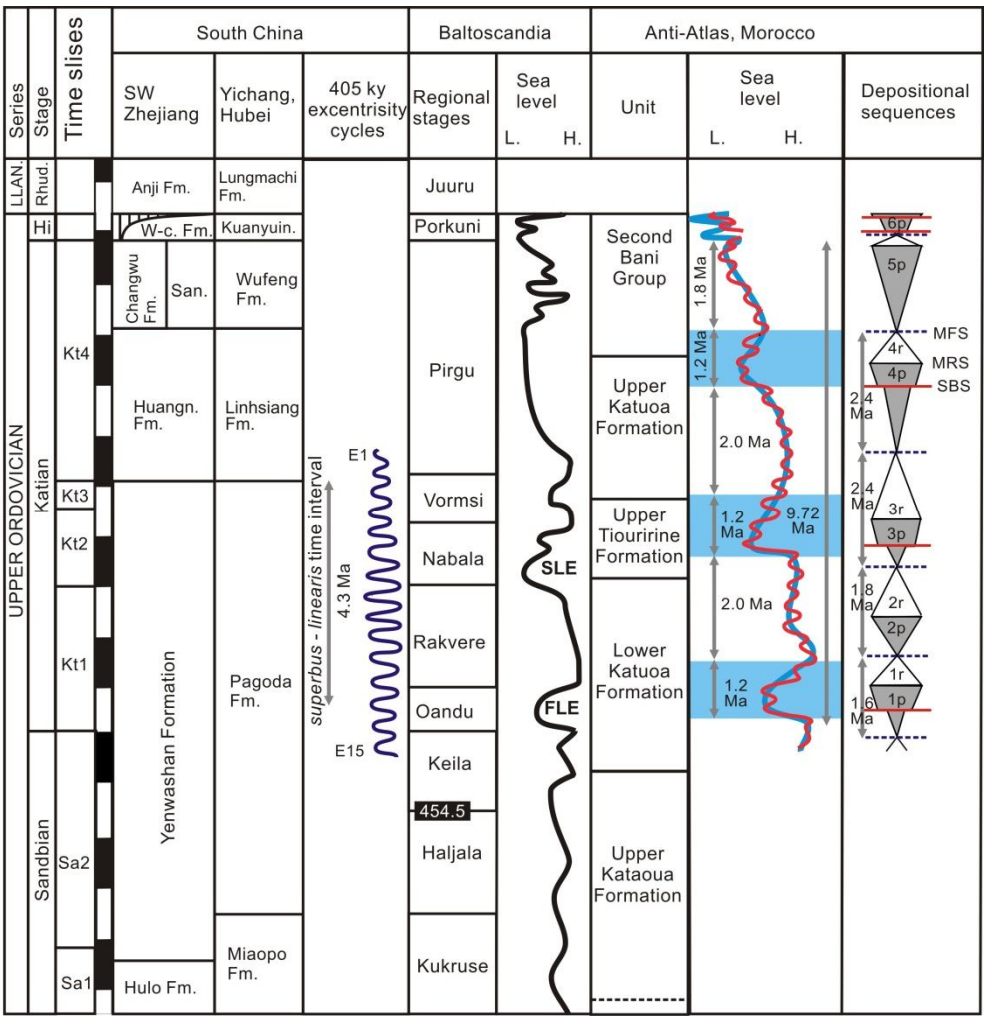

Figure 2 (continued). Cyclostratigraphy of Pagoda and Linhsiang Formation is after Zhong et al. (2018); sea level curve for upper *elongata* chitinozoan Zone (Figure 2a). Ordovician of Baltoscandia after Nielsen et al. 2004, SLE – Solvang L.E., FLE – Frognarkilen Lowstand Event; inferred 405 ky 1.2 Ma and 2.4 Ma sedimentary cycles and depositional sequences for Upper Ordovician of Morocco after Loi et al. 2010. Inferred numerical ages of the stage and graptolite zonal boundaries shown in Ma. Position of possible cooling intervals is shown by blue strips.

North Africa

It is possible to anchor the Upper Ordovician Katian to Hirnantian succession at Bou Ingarf in the Anti-Atlas, Morocco against the radio-isotope dated Katian/Hirnantian and Ordovician/Silurian boundaries is reconsidered. This stems from the significantly shorter duration for the Hirnantian suggested by recent high-resolution dating (0.47 ± 0.34 Ma; Ling et al. 2019) compared with previous estimates, including by Loi et al. (2010). Those authors placed the lower Hirnantian boundary in the lower part of the Lower Second Bani Formation. slightly above the The major Hirnantian lowstand, as it is shown by Loi et al. (2010; Figure 5), is confined to the uppermost part of the Upper Second Bani Formation and is correlated with the major and very short lived glacial event in North Africa (Loi et al. 2010, Figure 13). It most probably coincides with the whole Hirnantian Stage as formally defined (Chen et al. 2006). The implication is that the Lower Second Bani Formation and a significant part of the *elongata* Zone belong to the latest Katian. With addition of the three genetic fourth-order sequences corresponding to the Lower Second Bani Formation, the estimated duration of the Katian Stage at Bou Ingarf would be c. 10.1 Ma (total 25 generic sequences), which fits closely with the new estimates of the Katian Stage duration as c. 10 Ma based on high resolution radio-isotope ages (Ling et al. 2019; Metzger et al. 2020). Cycle 15 (Videt et al. 2010) could be indicative for the lowermost Katian Stage.

The Katian sedimentary record presented by Loi et al. (2010) suggests three episodes of major sea-level lowstand with duration of c. 1.2 Ma (three genetic sequences) separated by highstand intervals c. 2.0 Ma long (Figure 2). Sea-level falls were linked to the significant glacio-eustatic oscillations caused by amalgamation and growth of terrestrial ice shields in African Gondwana (Loi et al. 2010; Figure 14); however, the global correlation they proposed requires reconsideration. The timing of the lowermost abrupt regression and lowstand documented at Bou Ingarf can be estimated as 452.4–451.2 Ma based on the age calibration for the Katian/Hirnantian boundary (Ling et al. 2019). This correlates in Laurentia (Holland and Patzkowsky 1998; Figure 2a) with lowstand (sequences M5 and M6) followed by a significant transgressive event (at the base of the sequence C1) and preceded by the GICE negative carbon isotope excursion. In Baltoscandia a widespread hiatus documented within the Oandu Regional stage (Frognarkilen Lowstand Event of Nielsen 2004) follows the GICE interval at the Keila/Oandu boundary (Bergström et al. 2010, 2015; Figure 2b FLE).

The mid Katian sea-level lowstand at 449.6–448.2 Ma* (*fistulosa – barbata* chitinozoan zones; *ages given follow the cyclostratigraphic successions of Loi et al. 2010 and Dabard et al. 2015) can be correlated with the lower part of the *linearis* graptolite Biozone. In Baltoscandia, a pronounced sea level lowstand in the lower part of the Nabala Regional Stage (Figure 2b SLE), and related palaeokarst at the top of the Slandrom Limestone, are somewhat below the Saunja (=Waynesville; Figure 2a) positive carbon isotope excursion (Ainsaar et al. 2004; Calner et al. 2010). Transgressive black shales of the overlying Fjäcka Formation contain graptolites characteristic of the *linearis* Zone. Bergström et al. (2010, 2015) correlated this lowstand interval with the Mayswillian (sequences C2 and C3 of the Cincinnati Region) in Laurentia (Figure 2a). The following flooding event in the lower part of the *nigerica* chitinozoan Biozone most probably occurred synchronously with the basal Richmondian transgression in Laurentia.

The late Katian sea-level lowstand dated 446.1–444.9 Ma* corresponds to the uppermost parts of the *complanatus* graptolite Zone and *merga* chitinozoan Zone (Figure 2a). In Baltoscandia this may correlate not with the Husbergøya Lowstand Event of Nielsen (2004) but rather with the unspecified regression and associated hiatus at the base of the Adila and Kuldiga formations traceable in Estonia and Latvia (Nielsen 2004, Figure 10.2; Hints et al. 2005). A succeeding flooding event at the base of the *anceps* graptolite Zone, dated by Ling et al. (2019) as 444.84 ± 0.31 Ma*, closely corresponds with wide dispersal of the early pentameridine and atrypidine brachiopods, which first appeared about that time at South China, Baltica and Laurentia (Popov et al. 1999; Harper et al. 2013).

Longer orbital cyclicity at Bou Ingarf is less clear. The duration of the third and fourth third-order sequences may be linked to the c. 2.4 Ma g4–g3 eccentricity cycle (Laskar et al. 2004, 2011) although the first and second sequences are shortened to 1.6 Ma and 1.8 Ma respectively (Figure 2b). One explanation is this could be a sign of the chaotic diffusion of the planetary orbits (Laskar et al. 2004) but it requires further study. Also, the six third-order sequences linked to the Hirnantian glaciation do not fit into the observed pattern (Figure 2b), which may suggest that factors other than orbital forcing had a substantial impact on climate at that time.

West Brittany. The almost continuous Darriwilian to Sandbian cyclostratigraphical record represents a well-documented succession of third- and fourth-order sequences in the Crozon Peninsula of the Armorican Massif (western France), which was a part

of Mediterranean Gondwana at that time (Dabard et al. 2015; Figure 1). In addition to detailed sedimentological analysis, the study is supported by a gamma-ray record. The cyclostratigraphical scale is difficult to correlate with stage boundaries because of the absence of biostratigraphically indicative graptolite taxa and the lack of reliable radio-isotope ages within that time interval. However, a significant drowning event and discontinuity occur at the base of the Kemeur Formation, which contains chitinozoans of the *tanvillensis* Zone indicative for the lower Katian (Figure 1). This is most probably the same sea-level fall as is documented within the sequence O11 in North African Gondwana (Videt et al. 2010), including the first Katian regressive event at the section of Bou Ingarf where it has been dated as 452.4–451.2 Ma* (Figure 2b). In the Crozon Peninsula succession, the base of the Katian Series (453.12 ± 0.38 Ma) can be provisionally placed at the level of two genetic sequences below the Kemeur Formation (Figure 1C). The base of the Sandbian Stage should be placed somewhere in the upper part of the *pissotensis* chitinozoan Zone, but in the absence of the biostratigraphically indicative graptolites its position cannot be defined with satisfactory precision. The same is true for the lower Darriwilian boundary, which is placed conditionally in the upper *henryi* chitinozoan Biozone (Ogg et al. 2016). According to Dabard et al. (2015) there is a continuous Dapingian to Darriwilian transition in the Crozon Peninsula section, while the age calibrated duration of the *henryi* and *bulla* biozones is very short and does not exceed 100 ky for each. Hence, the position of the lower Darriwilian boundary at the base of the 4 m thick unit within the total range of these two biozones can be taken with some confidence. Those results in an estimated duration for the Darriwilian plus Sandbian of c. 13.8 Ma with one genetic sequence probably lost (on the top of PC8; Dabard et al. 2015, p. 108). That duration is closely similar to the 14.2 Ma inferred by Ogg et al. (2016; Figure 1). In the absence of biostratigraphically informative conodonts and graptolites, a direct high-resolution biostratigraphical correlation of the Darriwilian to Sandbian succession of Armorica with those outside the 'North Gondwana' domain (e.g. Baltica, Laurentia and South China) is impossible, as is direct correlation with the carbon isotope curve.

The Crozon succession of W Brittany is dominated by 1.2 Ma third-order sequences, which may be linked with long-period obliquity cycles. Two sequences (PC2 and PC9) have a longer duration of c. 2 Ma. Two major flooding events, known as the *formosa* and *pissotensis* events based on chitinozoan stratigraphy (Paris et al. 2007), are documented near the bases of the Corréjou and Morgat members respectively (Figure 1C). These are widely recognised from a number of sections within the Mediterranean, North African and Arabian sectors of Gondwana (Dabard et al. 2015 and references therein).

The biostratigraphical age constraints for the younger, *pissotensis* Flooding Event are difficult due to the long duration of the *pissotensis* Zone. However, it was preceded by three successive short-lived sea-level falls of significant amplitude (50–80 m) confined to a c. 1.2 Ma time interval (Figure 1C; sequence Ps9, lower part), ascribed most probably to glacio-eustasy by Dabard et al. (2015). The 464.7–465.9 Ma* age estimated for this cooling, based on correlation of the cyclostratigraphical sequences of Bou Ingarf and Crozon, as explained above, means it was probably within the time interval corresponding to the upper *serra* and lower *anserinus* conodont zones (Figure 1). The scale of successive sea-level falls (> 150 m) during that interval suggests that it should be recorded in the contemporaneous sedimentary record of other continents, yet in Baltoscandia Nielsen (2004) recognized a pronounced highstand interval (Furudal Highstand; Figure 2b). In South China a significant hiatus is present at least in some sections in the upper part of the Darriwilian. In particular, a substantial gap between the Gunitan and Datianba formations in Hunan province is topped by a disconformity with a significant part of the *suecicus* and *serra* conodont zones missing (Zhang 1996; Holmer et al. 2017). Overlying intercalated shales and marls of the Miaopo Formation contain conodonts of the uppermost Darriwilian to lower Sandbian *anserinus* Biozone at the base, which represents a major flooding surface and significant drowning event.

The older, *formosa* Flooding Event can be correlated with the Shelve area of the UK, at that time part of Avalonia, since *formosa* chitinozoans are documented from the upper part of the *artus* graptolite Zone (Hope Shale Formation, lower Abereiddian), which allows correlation with the *pseudoplanus* conodont Biozone, as well as with *lentus* and the lower *fasciculatus* graptolite zones of Baltoscandia (Bergström et al. 2010). It was also preceded by a conspicuous short-term and high amplitude sea-level fall (Figure 1C). That may suggest correlation of the *formosa* Flooding Event with the Basal Llanvirn Drowning Event of Nielsen (2004) in the lower *Asaphus raniceps* Zone of Baltoscandia (Rasmussen et al. 2009). This horizon is slightly below the onset of the middle Darriwilian $\delta^{13}C$ excursion in Baltoscandia and South China (Schmitz et al. 2010; Figure 1).

From the reconstructed sea-level curve (Dabard et al. 2015, Figure 2b) it looks likely that the onset of a general regressive trend and associated cooling of the climate took place two genetic sequences earlier, when it was probably not associated with substantial ice sheet growth. Thus the Mid Darriwilian (MDICE)

negative carbon isotope excursion is possibly entirely .confined to the warmer interval between two major cooling events (Figure 2a). Another cooling event of similar duration can be dated as 464.7–465.9 Ma* in the late Sandbian, upper Kerarmor Member; however, poor biostratigraphical age constraints preclude tracing elsewhere with any degree of precision.

Arabian sector of Gondwana

A relatively continuous sedimentary record of 3rd and 4th order sea level fluctuations was presented by Turner et al. (2012) for the Hiswah and Dubaydib formations of southern Jordan at the Arabian sector of Gondwana (Figure 1D). The reconstructed succession of sedimentary sequences is based on the analysis of siliciclastic sediment stacking patterns. The authors argued that 24 genetic sequences documented from these units represent 405 ka orbital eccentricity cycles; sequences controlled by ~ 1.2 Ma obliquity and ~ 2.4 Ma eccentricity cycles were also recognised. At the base of the Hiswah Formation, a rapid rise in sea level is indicated by deposition of graptolite-bearing fine clastic sediments on fluvial sandstones assigned to the Umm Sahm Formation. The graptolites from the lowermost Hiswah Formation were recently re-assessed and assigned by Maletz (in Meischner et al. 2019) to *Didymograptus murchisoni* (Beck in Murchison 1839). In the Armorican Massif this species appears in the upper half of the Corréjou Member; hence the flooding event in southern Jordan is not synchronous with that at the base of the Corréjou Member at Crozon. Re-aligning the base of the Jordanian succession to the base of the *murchisoni* graptolite Zone (Ogg et al. 2016; Figure 1), the alleged glacial interval between Turner et al.'s (2012) sequence boundaries 3 and 4 comes coincidentally to lie in the sea level lowstand preceding the *pissotensis* Flooding Event in the Crozon section (Figure 1C, D). Characters of the third-order sequences also look broadly similar, but precise comparison is difficult in the absence of good biostratigraphical constraints. Similar revised correlation of the Jordanian sequences with the International Chronostratigraphical Time Scale was suggested earlier by Al-Husseini (2018, Figure 4).

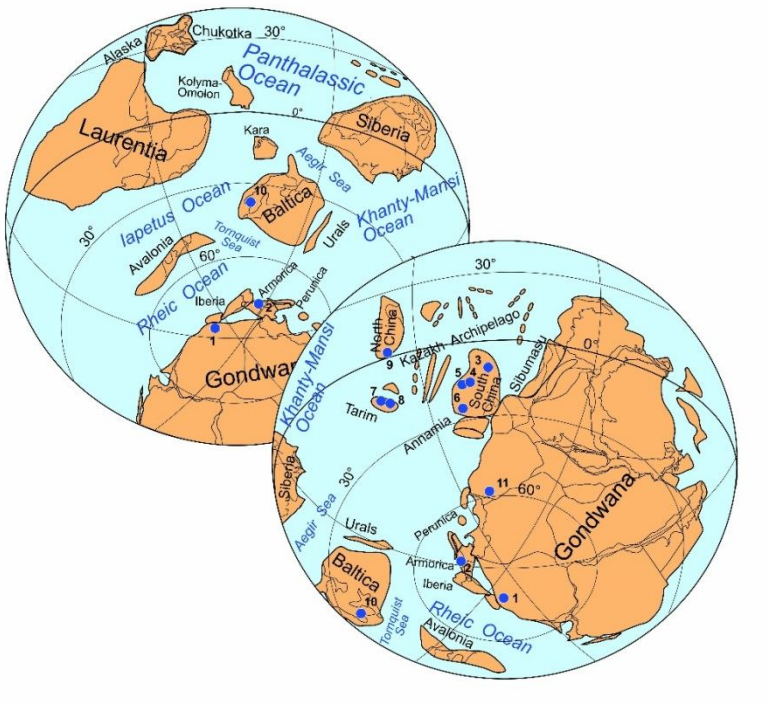

Figure 3. Global palaeogeographical reconstruction for the Sandbian showing locations of sections discussed: 1, Bou Ingarf in the Anti-Atlas, Morocco (Loi et al. 2010); 2, Crozon Peninsula, West Brittany, France (Dabard et al. 2015); 3, Huangnitang, South China (Zhong et al. 2018); 4, YH-1 borehole, Ychang, South China (Zhong et al. 2019); 5, EHD1 borehole, Ychang, South China (Zhong et al. 2020); 6, Wanhe, Yunnan, South China (Lu et al. 2019); 7, Dawangou, Tarim Fang et al. (2019); 8, Yangjikan, Tarim (Fang et al. 2019); 9, Guanzhuang, Ordos Basin, North China (Fang et al. 2016); 10, Oslo Region, Norway (Svensen et al. 2015), 11, Southern Jordan (Turner et al. 2012).

South China

The only comparable cyclostratigraphical record covering the Floian to Hirnantian stratigraphical interval is documented for the South China Continent (Zhong et al. 2018, 2019, 2020; Lu et al. 2019; Figure 1F). From stratigraphical profiles, data from time-series analyses of magnetic susceptibility, natural gamma-ray intensity and stable oxygen isotope relative values were used to extract sedimentary cycles linked to the 405 ky orbital eccentricity cycles as well as to the long-term 1.2 Ma obliquity and 2.4 Ma eccentricity cycles. In the absence of reliable radio-isotope ages for that interval, observed successions were anchored against the available biostratigraphical markers. During the Ordovician, South China together with Annamia was part of a small continent that drifted north-east along the west Gondwana margin, lying within southern temperate latitudes during the Early to Middle Ordovician, but drifting into the southern subtropics by the end of the Ordovician Period (Cocks and Torsvik 2013; Popov and Cocks 2017; Figure 3). The Ordovician conodont and graptolite based biostratigraphical succession of South China is well constrained against the Global Chronostratigraphical Scale; the GSSP sections for the Dapingian, Darriwilian and Hirnantian stages are located in South China. Moreover, Ling et al.'s (2019) high resolution radio-isotope ages for biostratigraphically well-constrained upper Katian and Hirnantian K-bentonites in SW China established precise estimates for the duration of the Hirnantian Age, as well as dating the lower boundaries and duration of the *Dicellograptus complexus*, *Paraorthograptus pacificus*, *Tangyagraptus typicus*, *Metabolograptus extraordinarius* and *Metabolograptus persculptus* graptolite zones. These dates are potentially the key for the anchoring of the floating astrochronological time scales.

The astrochronologically calibrated cyclostratigraphical scale developed by Zhong et al. (2018) for the Huangnitang section at Changshan, Zhejiang Province is of special interest because it can be anchored against the GSSP of the Darriwilian Stage defined by FAD of *Undulograptus austrodentatus* Harris and Keble, 1932 (Figure 1). The section is located close to the outer margin of the Jiangnan Slope Belt (Chen et al. 2006), representing a transition from the outer shelf to upper slope lithofacies. In the lower part of the succession, the Ningkuo Formation comprises black shales with subsidiary limestone beds, probably representing distal tempestites; its age span from *austrodentatus* to *ellesae* graptolite zones is supported by the occurrences of the index-species. The upper part of the succession is the Hulo Formation, comprising mainly limestones with intercalated graptolitic shales. Conodont and graptolite biostratigraphy adopted by Zhong et al. (2018) is based on data presented by Chen et al. (2006). The section was *a priori* considered as a complete representation of the Darriwilian Stage, without significant gaps and interruptions. The study was apparently not supported by detailed sedimentological observations, therefore the possibility of condensed intervals and cryptic unconformities, which are relatively common in such depositional environments (e.g. Trabucho-Alexandre 2014), was not taken into consideration. Munnecke et al. (2011, p. 39) queried but could not account for the lack of indication of the MDICE isotope event in the Huangnitang section. Zhong et al. (2018) had proposed that times of minimum insolation and cooler climate resulted in weaker runoff and hence reduced magnetic mineral input into the ocean. This explanation ignores a perhaps more likely process, (for alternatives processes see Ellwood et al. 2013, p. 344), notably, that progressive loss of ferromagnetic materials originally incorporated into soft sediment took place shortly after burial and during subsequent diagenetic processes mainly due to bacterial activity, which is especially characteristic for the redox environment typical of graptolitic shales (Ellwood et al. 1988).

The assessed duration of the Darriwilian Stage obtained from the Huangnitang section is 8.38 ± 0.4 Ma (20 eccentricity cycles), which is slightly shorter than the estimate (8.9 ± 0.9 Ma) given by Ogg et al. (2016; Figure 1). However, a significant discrepancy is evident in a very short duration for the *fasciculatus*, *elegans* and '*teretiusculus'* zones, which together do not exceed c. 1.5 Ma (Figures 1, 4). It prompts detailed discussion of the graptolite and conodont biostratigraphical record presently available, and notably none of the nominal species of these three biozones have been documented from that section. The presence of the *fasciculatus* Zone equivalent is based on a rich graptolite assemblage. The correlation of the *elegans* Zone looks less certain. Its lower boundary is placed at the base of a thin shale layer sandwiched between two limestone beds (Chen et al. 2006, Figure 2, samples 261, 11114h) that contains a rich graptolite assemblage including 15 taxa transitional from the underlying units. The limestone bed overlying the shale layer (Chen et al. 2006, Figure 2, sample 11115wg) contains a conodont assemblage including *Lenodus* cf. *pseudoplanus* (Viira, 1974), *Histiodella holodentata* Ethington and Clark, 1981 and *H. kristinae* Stouge, 1984, the last of which has a narrow total range within the upper *pseudoplanus* (*ozarkodella* Subzone) to the lowermost *suecicus* Zone (*lunensis* Subzone) (Zhang 1998; Mestre and Heredia 2012). Although in Baltoscandia *H. kristinae* possibly overlaps slightly with the range of the graptolite *Pterograptus elegans* Holm, 1881, the latter according to Bergström et al. (2018) first appears in the lower part of the *suecicus* Zone (*lunensis* Subzone) (Figure 4). Co-occurrence

of *H. kristinae* and *H. holodentata* is documented only in the upper *pseudoplanus* Zone and the former species does not indicate the base of the *serra* Zone (Mestre and Heredia 2012). It leaves little doubt that the base of the *elegans* Zone should be placed higher up-section, but it cannot be identified with precision in the absence of the index-taxon. The so-called '*teretiusculus'* Zone is in fact the interzone, which contains neither graptolites nor conodonts. The graptolites re-appear at the top of the Darriwilian succession in the lower part of a 1.7 m thick shale unit (Chen et al. 2006; Figure 2, sample 262), where in the lowest sample of three species, two are transitional to the *gracilis* Zone assemblage, and this Zone is documented from the next higher sample (Chen et al. 2006; Figure 2, sample 263) within the same shale unit. The base of the shale bed may represent a flooding surface, but it is obscured by the underlying volcanic rocks and requires sedimentological study.

The biostratigraphical constraints of the Huangnitang section are not satisfactory to confirm the continuous character of the succession. Rather, the short time duration of the stratigraphical interval above the occurrence of *H. kristinae* together with the absence of any evidence of the MDICE stable isotope excursion, suggests a major hiatus in the upper part of the Darriwilian, probably, corresponding to a significant part, if not all, of the *serra* Zone and the lower *anserinus* Zone. A comparable hiatus was documented by Zhang (1996, 1998) and Holmer et al. (2017) for the Maocaopu section located in the inner part of the Jiangnan Slope Belt.

Further evidence comes from comparison of the astrochronological record obtained by Fang et al. (2019) for the upper Darriwilian Saergan Formation of Tarim, NW China (Figure 1E). The lower boundary of Saergan Formation black shales with thin limestones is laterally discontinuous (Zhang and Munnecke 2016, Figure 2), while graptolites of the *elegans* Zone first appear at the base of the formation (Chen et al. 2012). This implies correlation with the upper part of the Hulo Formation above the fossiliferous horizon containing *H. kristinae* at Huangnitang. The cyclostratigraphical profile obtained by Fang et al. (2019) for the Saergan Formation of Tarim includes 9 genetic 405 ky sequences from the base of *elegans* up to the base of the *gracilis* Zone (Figure 1E) suggesting 3.65 Ma as a likely duration for deposition of the unit. This compares with the 4.2 Ma estimate for the upper Darriwilian Dw3 time slice (base of *serra* to base of *gracilis* zones) made by Ogg et al. (2016; Figure 1), and is also relatively well constrained biostratigraphically to the *serra* and lower *anserinus* zones. It significantly exceeds c. 0.9 Ma inferred by Zhong et al. (2018, Figure 8) for the interval from the base of *elegans* to the base of *gracilis* Zone. The only plausible explanation is a major unrecognised unconformity in the Huangnitang section.

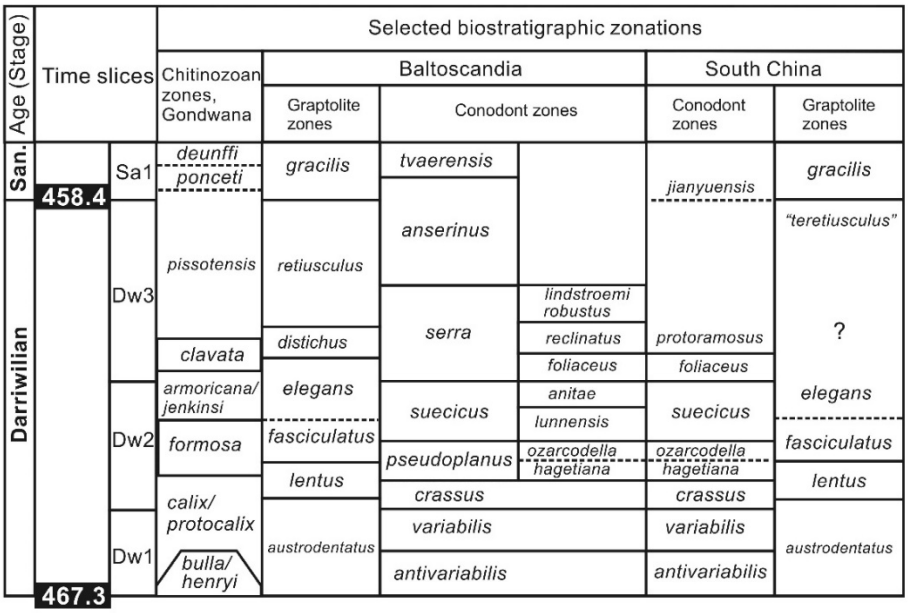

Figure 4. Correlation chart of the Darriwilian conodont and graptolite zones of South China and Baltoscandia, mainly after Bergström et al. (2018) and Chen et al. (2011). Darriwilian Stage time slices after Copper et al. (2012). Chitinozoan biozones of Mediterranean Gondwana (for reference) after Paris (1990) and Paris et al. (2007).

The occurrence of the conodont *H. kristinae* in the uppermost Hulo Formation Member 1 at Huangnitang, indicating the upper *pseudoplanus* Biozone, suggests a relatively precise correlation with the *formosa* chitinozoan Zone (Figure 4). It also enables comparison with the cyclostratigrapical successions developed for the Darriwilian of South China and the Armorican Massif (Figure 1). At Crozon, the stratigraphical interval from the base of the *formosa* Zone down to the inferred base of the Darriwilian Stage is c. 2 Ma, comparable to Ogg et al. (2016; Figure 1). According to Zhong et al. (2018), the equivalent interval from the *H. kristinae* horizon (upper *pseudoplanus* Zone) down to the FAD of *Undulograptus austrodentatus* at the base of the Darriwilian includes 18 genetic sequences with an estimated time span of c. 7.3 Ma. This exceeds by more than three and half times the estimate from the Crozon Peninsula section (Dabard et al. 2015). Adding the < 2 Ma estimated for the upper Darriwilian by Fang et al. (2019) for the Hulo Formation, the duration of the Huangnitang Darriwilian will increase to 11 Ma, well above the 8.9 Ma of Ogg et al. (2016; Figure 1). The most likely explanation for the observed discrepancy is an erroneous interpretation of the cyclostratigraphical signal obtained by Zhong et al. (2018) from the Huangnitang section, due to the lack of close sedimentological control, and an erroneous assumption that the Darriwilian succession is complete. Possibly, the signal picked up may represent the basic c. 100 ky eccentricity cycles with a few lost due to cryptic disconformities and condensed intervals. Because of obvious problems, we suspend discussion of the Floian – Darriwilian cyclostratigraphical profile obtained by Zhong et al. (2018) from the core of CJ-3 bore-hole.

Another astrochronologically calibrated cyclostratigraphical scale is proposed by Zhong et al. (2019) for the upper Sandbian to lower Katian stratigraphical interval. Similar methodology (magnetic susceptibility, natural gamma-ray intensity and stable oxygen isotope relative values from stratigraphical profiles) was used to study the Pagoda and Linhsiang formations obtained from YH-1 borehole located near Ychang city, Hubey Province, on the Yangtze Platform (Figure 2b). The sampled bore-hole core (YH-1) represents a monotonous succession of the intercalated light grey and purplish red limestones. The approximate position of the *superbus* and *insculptus* conodont zones, and the lower boundary of the *complanatus* graptolite Zone (Figure 2b) are indicated, although the biostratigraphy is not discussed nor criteria used to define biostratigraphical boundaries. The lower boundary of the Linhsiang Formation, where there is no visible lithological change, is placed at the base of the *insculptus* conodont Zone (Zhong et al. 2019, Figure 4). Unfortunately, the biozonation shown erroneously mixes graptolites and conodonts, while existing correlation charts (e.g. Zhang et al. 2019, Figure 5) show the base of the Linhsiang coincident with the lower boundary of the *complanatus* graptolite Zone (Figure 2b; *insculptus* = *ordovicicus*). Due to the absence of clearly defined biostratigraphical boundaries the proposed cyclostratigraphical scale should be formally considered as unrooted; nevertheless, c. 4.3 Ma for the stratigraphical interval between the inferred base of *superbus* and *complanatus* zones (Figure 1) compares well with Ogg et al. (2016; Figure, 2b).

Lu et al. (2019) and Zhong et al. (2020) described late Katian to Hirnantian cyclostratigraphy based on stratigraphical successions in the Wanhe section (Lianfeng, Yunnan Province) and the EHD1 borehole north-west of Ychang (Upper Yangtze area) (Figure 5). Both sections exhibit a continuous succession of graptolite zones from *complexus* (late Katian) to *persculptus* (Hirnantian). The upper Katian – lower Hirnantian (*complexus* – *extraordinarius* zones) Wufeng Formation of the EHD1 borehole is organic-rich mudstones, while the Daduhe Formation of Wanhe is black shale and dark-grey calcareous mudstone with limestone intercalations. In both sections the Ordovician succession is topped by the Longmaxi Formation of grey to black silty shales continuous up into the Rhuddanian (Figure 5). The Longmaxi Formation rests on a shell bed, the Guanyinqiao Bed in EDHI, and the Kuanyinchiao Formation (< 0.5 m) at Wanhe (Ling et al., 2019). This event horizon marks the boundary of *extraordinarius* and *persculptus* graptolite zones, the latter marked by proliferation of the *Hirnantia* Fauna.

The astronomical calibration of the cyclostratigraphical succession in both publications (Figure 5) is problematical because it assumes the duration of the Hirnantian Stage as c. 1.33 Ma (Cooper and Sadler 2012). Ling et al. (2019) convincingly demonstrated a much shorter duration for the Hirnantian Stage (c. 0.47 ± 0.34 Ma) based on high resolution radiogenic isotope dating from four successive bentonite beds (*complexus*, *typicus* and *extraordinarius* graptolite zones) at the Wanhe section.

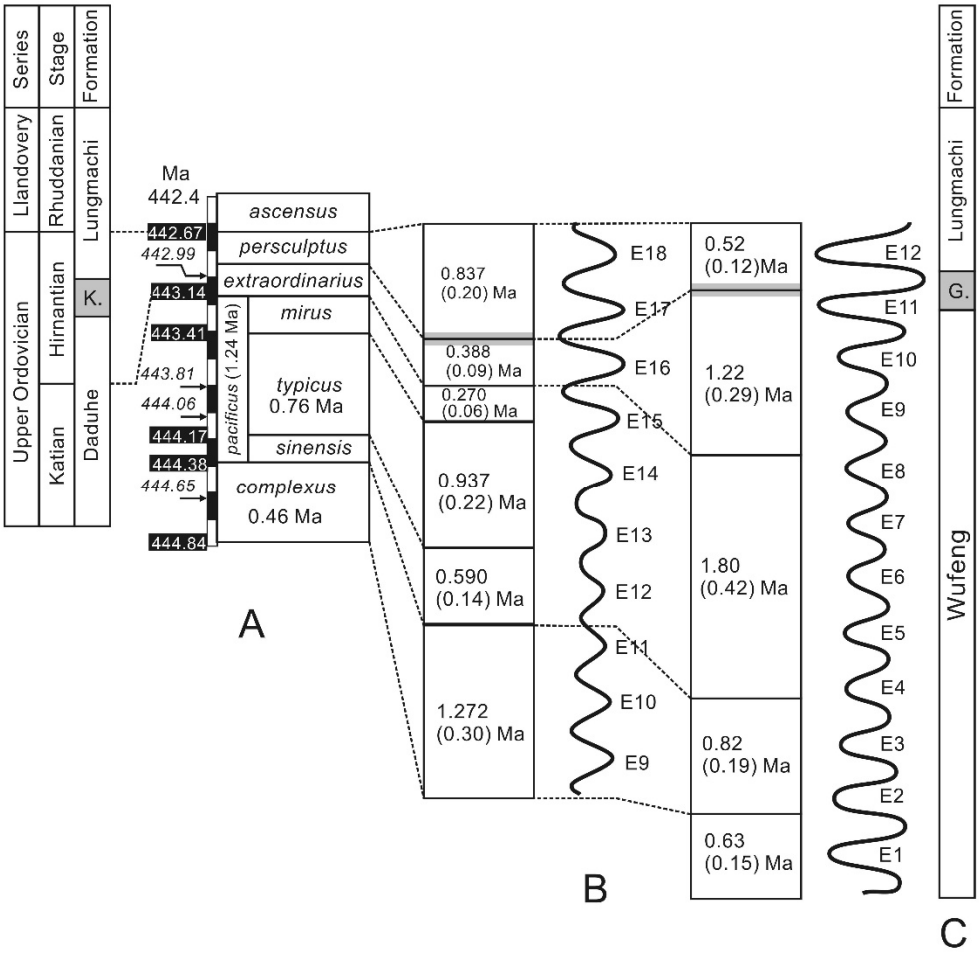

Figure 5. A Estimated numerical ages of stage and graptolite zonal boundaries and U-Pb isotope ages (shown in Italics) for bentonite beds used for dating Wanhe section (after Ling et al. 2019). **B** Astronomically calibrated durations of the graptolite zones and inferred 405 ky long-eccentricity cycles at the Wanhe section (Zhong et al. 2020). **C** Estimated duration of late Katian to Hirnantian graptolite zones and inferred 'fourth-order' eustatic changes at EHD1 borehole section after Lu et al. (2019). Relative duration of graptolite zones based on alternative interpretation of the cyclostratigraphic sequence as succession of short term 95 ky eccentricity cycles shown in parentheses.

For the basal *complexus* – top *persculptus* interval, Lu et al. (2019) recognised 10 genetic sequences or c. 4.3 Ma in the Wanhe section while Zhong et al. (2020) have 11 genetic sequences or 3.8 Ma for the EHD1 borehole section (Figure 5). If, however, each genetic sequence represents a 405 ky eccentricity cycle, these overestimate greatly the c. 2.17 Ma duration for this stratigraphical interval (obtained by Ling et al. (2019). The age estimates for the Hirnantian Stage (c. 1.235 Ma for the Wanhe section, 1.74 Ma or four genetic sequences for the EHD1 borehole) require review. The most plausible explanation of the observed discrepancy is that the orbital eccentricity cycles presented by Lu et al. (2019) and Zhong et al. (2020) are in fact short term eccentricity, either 95 ky or 128 ky cycles. If, as Fang et al. (2016) considered, they represent 95 ky eccentricity cycles, the duration of the *extraordinarius* Zone in the EHD1 borehole section approaches 0.29 Ma, while the *persculptus* Zone in the Wanhe succession is c. 0.2 Ma, in total 0.49 Ma which lies well within the Ling et al. (2019) estimates. It would also imply that the Katian sedimentary record of both successions is incomplete, with around half the total 95 ka obliquity cycles lost due to cryptic disconformities and condensed intervals as is not unusual in epicratonic shale successions (e.g. Trabucho-Alexandre 2014). This would leave the supposed third order sequences in both sections most likely to reflect long term 405 ka eccentricity cycles, not 1.2 Ma obliquity cycles as originally expected, but these are also incompletely preserved.

Tarim and North China

Astronomically calibrated cyclostratigraphical records are currently published for the Darriwilian of Tarim (Fang et al. 2019) and Sandbian of North China (Fang et al. 2016). At those times, Tarim was a microcontinent located in southern tropical latitudes, while North China is considered as an isolated small continent located in the northern subtropics (Popov and Cocks 2017; Figure 3). Both lay in relative proximity to the western coast of equatorial Gondwana and occupied a position peripheral to the Kazakh Archipelago, which was a major Late Ordovician biodiversity hot spot (Popov and Cocks 2017). North China is especially interesting because it is the only palaeocontinent located entirely in the northern hemisphere that has a documented Ordovician astronomically calibrated cyclostratigraphical record, entirely confined to the Sandbian Stage (Fang et al. 2016). Sedimentological study of the Pingliang Formation at the Guanzhuang section was supported by a cyclostratigraphical profile based on magnetic susceptibility. The Guanzhuang section is located on the southwestern margin of the Ordos Basin, North China. The Pingliang Formation comprises rhythmic alternations of shales and limestones with subsidiary cherts, deposited on the slope of a convergent continental margin (Song et al., 2013). It contains rich graptolite, conodont and radiolarian faunas (Wang 1993; Finney et al. 1999; Wang et al. 2013) and for some time was considered as a candidate for the GSSP for the Sandbian Stage (Finney et al. 1999). The 35 m thick interval covered in the cyclostratigraphical analysis by Fang et al. (2016) corresponds to the *variabilis* and *gerdae* subzones of the *tvaerensis* conodont Zone (Figure 1); however, in the absence of the nominal species the approximately defined boundaries of these units cannot be considered suitable for anchoring an astrochronological time scale. In spite of this, the estimated duration of these conodont zones (3.38 Ma) is in a good agreement with Ogg et al. (2016). Unfortunately, the Darriwilian/Sandbian boundary interval was omitted from the Fang et al. (2016) cyclostratigraphical analysis, probably due to the high proportion of carbonate rocks in the succession. The presence of bentonite beds makes the Guanzhuang section potentially important for time calibration of the *aculeata* and *quadridactylus* conodont zonal boundaries.

Fang et al. (2016) recognised long eccentricity cycles of c. 400 ky 760 ky and 2040 ky based on modulation of the basic 95 ky signal. They also linked characteristics of the Pingliang Formation sedimentation to low amplitude sea level fluctuations mainly controlled by precession cycles, typical for low latitudes, and suggested that glacio-eustasy was a driving force. These conclusions are in good agreement with Dabard et al. (2015), who inferred a significant late Sandbian cooling event not shown by the astrochronological record from the Pingliang Formation.

Fang et al. (2019) documented the astronomically calibrated cyclostratigraphical record for the Saergan Formation at Dawangou and the Dawangou Formation at Yangjikan, both in the north-western part of the Tarim Basin (Figure 1E). The Dawangou section was approved in 2001 as the auxiliary GSSP for the base of the Sandbian Stage and the Upper Ordovician Series. The Saergan Formation at Dawangou comprises a condensed succession of black calcareous graptolitic shales, 14 m thick, with a few limestone beds. It rests disconformably on limestones of the Dawangou Formation. The conodont biostratigraphy of the Darriwilian deposits at the Dawangou section was re-assessed by Zhen at al. (2011), while the graptolite biostratigraphy from *elegans* to *gracilis* zones was documented for the Saergan Formation by Chen et al. (2011). Fang et al. (2019) used magnetic susceptibility and gamma ray spectrometry with measurements taken directly in the field; however, there is no indication that the study was supported by detailed sedimentological observation necessary to consider possible hiatuses and condensed intervals.

A significant issue, unresolved in the paper, is the correlation presented for the Darriwilian successions at the two localities. The upper part of the Dawangou Formation at the Yangjikan section yielded conodonts of the *anserinus* and *jianyeensis* zones. However, biostratigraphically indicative conodont species for the upper *pseudoplanus* Zone are also recorded; *H. holodentata* first appears c. 6.5 m and *H. kristinae* c. 5.5 m below the top of the Dawangou Formation (Fang et al. 2019, Figure 3). *H. kristinae* has a narrow taxon-range zone, hence its FAD is used for anchoring astrochronological time scales, and the taxon-range zones of both species do not overlap with the *serra*, *anserinus* and *jianyeensis* zones. Remarkably, according to Zhen et al. 2011, in the type section of the Dawangou Formation at Dawangou, *H. holodentata* was first documented 6.5 m below the top, while *H. kristinae* occurred at the very top of the Dawangou Formation (Zhen et al. 2011, Figure 3), thus the uppermost parts of the Dawangou Formation at Dawangou and Yangjikan sections are almost certainly synchronous and there is no evidence of overlap with the Saergan Formation. Zhang and Munnecke (2016, Figures 2, 6) also suggested that the top of the Dawangou Formation in both sections is not younger than the lower part of the *kristinae* Zone, and there is then a significant gap corresponding to the entire *serra* Zone and the lower part of the *anserinus* Zone at the Yangjikan section. Thus the correlation between these two sections inferred by Fang et al. (2019, Figure 7) is firmly rejected here, which raises doubt about the proposed

timing of climatic changes for the Darriwilian. According to Zhang and Munnecke (2016) increasing $\delta^{18}O$ values that possibly correspond to the rising limb of the MDICE stable isotope event are documented for the uppermost Dawangou Formation (*kristinae* conodont Zone), while negative $\delta^{18}O$ values are characteristic for the Saergan Formation; indication of the falling limb of MDICE was probably lost in the hiatus.

The lower Darriwilian boundary in the Yangjikan section was conditionally placed at the base of the Dawangou Formation (Fang et al. 2019); however, this is not supported by the biostratigraphical evidence. If the cyclostratigraphcal succession of the Dawangou Formation is aligned against the FAD of *Histiodella kristinae*, i.e. close to the base of the *pseudoplanus* conodont Zone and *formosa* chitinozoan Zone (Figure 1), the inferred duration of the Darriwilian is about 4.9 Ma (12 generic 405 ky sequences), which is almost twice as large as estimated by Ogg et al. (2016) and Dabard et al. (2015). The observed discrepancy may be due to erroneous calibration of the astrochronological profile from the Dawangou Formation, stemming from the unsupported assumptions that the succession lacks hiatuses and corresponds to the entire Darriwilian.

The astrochronological profile obtained from the Saergan Formation for the upper Darriwilian is anchored to the base of the *gracilis* Zone and gives realistic estimates for the duration of the stratigraphical interval from the base of *elegans* to the base of *gracilis* Zone (Figure 1), yet it cannot be used for time calibration of the *serra* Zone due to the basal discontinuity and sporadic occurrences of the nominal taxon (Zhen et al. 2011).

Laurentia

Methods of high resolution sequence stratigraphy are widely applied to the Upper Ordovician succession of Laurentia (Holland and Patzkowsky 1996, 1998; Brett et al. 2020 and references herein) and a zonation based on $\delta^{13}C$ chemostratigraphy has been developed for the Dapingian – Hirnantian stratigraphical interval (Bergström et al. 2010, 2015; Figure 1B). By contrast to carbon isotope records from younger rocks, most notably the Cainozoic (Boulila et al. 2012), and with the exception of Cherns et al. (2013) and Al-Husseini (2016a, b), attempts to link observed patterns of Ordovician cyclicity to astrochronological cycles have been relatively few (e.g., Long 2007; Ellwood et al. 2013; Elrich et al. 2013; Hinnov and Diecchio 2015).

The pioneer study of astrochronological calibration of sedimentary cycles, on the Ordovician – Silurian boundary interval of Anticosti Island, Canada (Long 2007), was based on detailed sedimentological study of shallow marine deposits accumulated in a foreland basin setting on the eastern margin of the Laurentia continent at southern tropical latitudes (Figure 3). Sensitive proxy sea-level curves obtained from tempestite frequency analysis show distinct correlation with the inferred c. 100 ky and c. 400 ky orbital eccentricity cycles. A back-stripping procedure eliminated the effects of sediment loading, residual thermal and tectonically induced subsidence. Confusion over three–four? major peaks (Long 2007, H1–H4) in the Hirnantian Ellis Bay Formation arose mainly because of a strongly overestimated duration for the Hirnantian Stage (1.9 Ma) at that time. The recent reduction to 0.47 ± 0.34 Ma for the Hirnantian Stage based on high resolution zircon U–Pb ages (Ling et al. 2019) means that these peaks indeed most likely represent c. 100 ky short orbital eccentricity cycles. An important observation was that tempestite frequency curves do not correspond directly to sea-level curves generated using benthic communities, conodont assemblages, or sedimentary structures (Long 2007, p. 427), but are closely comparable to the predicted frequency of the short and long orbital eccentricity cycles.

Working on the Upper Ordovician of USA, Ellwood et al. (2013) tested the application of the magnetic susceptibility technique in astrochronological research against a well-studied marine shale and limestone succession. As well as extracting eccentricity cyclicities of c. 405 ky and c. 100 ky they identified obliquity c. 30.5 ky and c. 37.1 ky, and precession c. 19.3 ky cycles, they were also able to link these cyclicities to the characteristics of sedimentation visually on the outcrops. They stressed the importance of close biostratigraphical and sedimentological control in development of a chronostratigraphical framework, in order to reduce the impact of variable sedimentation rates and cryptic disconformities. The study represents an important step forward in building the late Ordovician astrochronological time scale based on data from low latitude, essentially carbonate successions.

Baltica

While possible effects of orbital forcing on the characters of sedimentation and biotic changes were discussed in several publications (e.g., Rasmussen et al. 2009; Egenhoff et al. 2010), only Svensen et al. (2015) specifically applied the magnetic susceptibility method to develop a cyclostratigraphy for the Baltoscandian Upper Ordovician succession. High resolution U–Pb zircon ages are given for the Kinnekulle K-bentonite and the base of the Keila Baltoscandian Regional Stage (454.52 ± 0.50 Ma). Three 405 ky long eccentricity cycles were recognised in the upper Arenstad Formation up to the boundary with the Frognerkilen Formation, while the peak of the GICE event is reported from the latter by Bergström et al. (2017). Metzger et al. (2020) recently reported high precision radiogenic ages for

the Deicke (453.35 ± 0.10 Ma) and Millbrig (453.36 ± 0.14 Ma) K-bentonites, and estimated onset of GICE at 453.21 ± 0.10 Ma with a duration not exceeding 400 ky It is in a good agreement with the duration of the upper part of the Arenstad Formation calculated astrochronologically by Svensen et al. (2015), but not with the age of the Sandbian/Katian boundary based on inferred average sedimentation rates.

Discussion

The cyclostratigraphical records developed by Loi et al. (2010) and Dabard et al. (2015) were secondary to the multi-order eustatic curves they produced based on detailed sedimentological studies. These studies demonstrated convincingly that the succession of 4th order sequences was controlled by well-expressed 405 ky orbital eccentricity cycles. Fifth-order sequences possibly linked with c. 100 ky eccentricity cycles, and sixth-order sequences possibly representing c. 20 ky precession, were also recognised.

Several patterns emerge from the eustatic/cyclostratigraphical curves presented. The Darriwilian - Sandbian interval is dominated by 1.2 Ma third order sequences (Figure 1), probably, reflecting the g4 − g3 obliquity modulation beat in the Laskar et al. (2004) eccentricity solution. Dabard et al. (2015) noted that this pattern is also characteristic for the Cainozoic icehouse sequences (e.g. Boulila et al. 2011), and they argued that ice sheets were present almost continuously in the southern hemisphere during Darriwilian – Sandbian times. Vandenbroucke et al. (2009, 2010) used early Sandbian chitinozoan distributions to argue for steep latitudinal faunal and temperature gradients in oceans of the southern hemisphere, resembling those of the present day, and indicative of pre-Katian oceanic cooling. Three intervals with duration c. 1.2 Ma are characterized by several large amplitude sea level falls (c. 50-80 m) and rapid water depth fluctuations (Figure 1C, arrowed), which may indicate major episodes of polar ice growth. Two of these are in the Darriwilian and are followed by the *formosa* and *pissotensis* flooding events of Paris et al. (2007); these can be recognised globally. The third, in the mid to late Sandbian, may correlate with a major lowstand documented by Holland and Patzkowsky (1998) in Laurentia but not yet recognised in Baltica and South China, probably because of poor biostratigraphical constraints. These cooling episodes are separated by prolonged intervals c. 4.1 – 4.5 Ma of warmer climates. The apparently shorter Sandbian cooling interval probably indicates a lost genetic sequence at Crozon at the Ps8/Ps9 sequence boundary (Figure 1C).

From higher palaeolatitudes, the cyclostratigraphical succession obtained for the Katian – Hirnantian of Morocco looks markedly different (Loi et al. 2010). The third-order sequences are characterised by $g_4 - g_3$ 2.4 Ma eccentricity cycle modulation, which is typical for Mesozoic greenhouse sequences according to Boulila et al. (2011). However, 2.0 Ma warm intervals were interrupted by substantial sea-level falls, corresponding to cooling episodes at c. 1.2 Ma and probably associated with substantial terrestrial ice sheet growth on Gondwana. The magnitude of sea-level falls at those times was probably greater than in the Darriwilian. Notably, in the Baltoscandian basin, Nielsen (2004) recognised the Frognarkilen Lowstand Event (Figure 2b FLE), which resulted in widespread unconformity at the Keilan – Oanduan transition, interpreted by Ainsaar and Meidla (2001) as a type 1 sequence boundary. It probably correlates with substantial sea-level fall followed by conspicuous flooding and associated with a high faunal turnover in Laurentia (Holland and Patzkowsky 1996, 1997; near the M4/M5 sequence boundary; Figure 2a). The mid Katian sea level fall corresponds in Morocco to the Upper Tiouririne Formation and *fistulosa – barbata* chitinozoan biozones, and is most probably synchronous with the Solvang Lowstand Event of Nielsen (2004; Figure 2b SLE) and widespread palaeokarst horizon at the top of Slandrom Limestone (Calner et al. 2010). The late Katian sea-level fall at the transition from the Upper Katuoa Formation to Second Bani Group is difficult to trace, probably because it is often amalgamated with the major unconformity of the terminal Ordovician glaciation in the southern hemisphere during the Hirnantian Age. It appears that the climate was in general considerably warmer in Katian than in Darriwilian – Sandbian times, but the cooling events were more frequent and more severe. Importantly, the two earliest Katian 3rd order sequences documented by Loi et al. (2010) are incomplete, each with only 4-5 genetic fourth order-sequences. It is possible that the early Katian interval coincided with a time of chaotic diffusion in the Earth orbital motion, which then changed to a new resonant state during mid to late Katian times (cf. Laskar et al., 2014, pp. 11-12). The Hirnantian glaciation and related sea level falls do not fit into the observed astrochronological pattern, which suggests that factors other than orbital forcing played an important role in triggering the terminal Ordovician ice age. In that respect comparative cyclostratigraphical studies of low latitude Upper Ordovician successions, e.g. Laurentia and Siberia, will be important to trace the impact of changing climate. In particular the well-studied Laurentian Upper Ordovician succession has good potential for the development of a reliable floating astrochronological scale. Its high-resolution sequence stratigraphical and biostratigraphical

frameworks, and the extensive nature of the Upper Ordovician outcrops, make it possible to build a reliable composite cyclostratigraphical succession based on magnetic susceptibility techniques (Ellwood et al. 2013; Brett et al. 2020).

It is well established for the Mesozoic and Cainozoic that $\delta^{13}C$ isotope signals carry a strong expression of the 405 ky orbital eccentricity cycles (e.g. Pälike et al. 2006), but these might also be seen in the Ordovician fourth-order eccentricity cycles. In addition, extremely long 9-Ma eccentricity cycles are expressed in the Cainozoic carbon isotope record (Boulila et al. 2012). There is an extensive record of carbon isotope geochemistry published for the Mid to Late Ordovician succession of Laurentia and Baltica (Ainsaar et al. 2010, Bergström et al. 2010; 2015). Yet, links between major Ordovician $\delta^{13}C$ excursions and global eustatic sea level changes remain somewhat uncertain. Bergström et al. (2010) noted that two of the Katian $\delta^{13}C$ excursions in Estonia occurred during sea level highstands and three during periods of relatively low sea level. In addition, correlation of the Katian sequence boundaries recognised in Baltica (e.g. Nielsen 2004; Dronov and Holmer 1999) and Laurentia (Holland and Patzkowsky 1996) often look problematic, which may suggest significant impact of local factors in inferred eustatic sea level curves. Revised sequence stratigraphy looks to have resolved this issue for Laurentia (Brett et al. 2020), yet it remains for Baltica. Notably, 16 fourth order sequences recognised by Brett et al. (2020) for the Upper Ordovician Mayswillian – Richmondian interval are the same number as for fourth order genetic sequences counted from the base of the Upper Tiouririne Formation to the base of Hirnantian in the Morocco Upper Ordovician succession (Figure 2b); possibly, not simply a coincidence. The Middle Ordovician sedimentary succession including the MDICE stable isotope excursion was covered in South China by Zhong et al. (2018) and Fang et al. (2019); however, both studies suffer through loss of critical stratigraphical intervals due to unrecognised discontinuities. Also, in the absence of relevant biostratigraphical and sedimentological support, it is impossible to compare patterns of the inferred Darriwilian climatic changes with the extensive sequence stratigraphical/cyclostratigraphical record of high latitude Gondwana (Dabard et al. 2015).

Matthews and Frohlich (2002) demonstrated that glacioeustatic signals linked to the 405 ky and 2.4 Ma can be seen even through the Mesozoic sequence stratigraphical record considered as representing a prolonged greenhouse time interval. Subsequently a model based on slight tuning of the Laskar et al. (2004) orbital solution predicted the ages of major sequence boundaries, lowstands and flooding events based on their inferred connection with the periodic astrochronological scale (Matthews and Al-Husseini 2010). The model included the significance of extremely long period cycles with durations of 14.58 Ma (Orbiton) and 28.37 Ma. Later, Al-Husseini (2016a, 2016b) applied this model to astrochronological interpretation of the global Ordovician sequence stratigraphical succession. At present, the documented Ordovician astrochronological record is too fragmentary and incomplete to verify those ideas, and hence we do not include detailed discussion here. Nevertheless, in a study that has no direct discussion of orbital forcing, Hammar (2003) pointed to the quasiperiodic nature of Baltoscandian biodiversity changes through the Ordovician, noting individual cycles of c. 12-14 Ma (~ orbiton of Matthews and Al-Husseini 2010) and with major biodiversity pulses in the late Tremadocian – early Floian (Billingenian Regional Stage, c. 480 Ma), mid Darriwilian (late Kundan Regional Stage, c. 465 Ma), and mid Katian (Nabala – Vormsi regional stages, c. 450 Ma). If compared with c. 29 Ma low amplitude periodicity calculated by Cherns et al. (2013, Figure 2) based on the distribution of the major climate indicators through the late Cambrian to Silurian sedimentary record, these pulses can be placed at the crest and two troughs of a single sine wave recalling a double Orbiton (28.37 Ma) of Matthews and Al-Husseini (2010). While the uncertainty interval in both cases looks high, it is likely that extremely low frequency, long obliquity cycle modulations were evident in the early Palaeozoic, and they might be represented in the biotic and geological record.

Conclusions

The astrochronologically calibrated sequence stratigraphical record of high latitude Gondwana (Loi et al. 2010; Dabard et al. 2015) shows significant impact from orbital forcing on the Mid to Late Ordovician climate, in particular, in the distinct and persistent high frequency glacio-eustatic signal recorded in fourth- to six-order sequences. It suggests also that the cooling trend through the Mid and Late Ordovician was significantly more complex than commonly envisaged. These data also draw into question the high tropical water temperatures inferred through the Early and Middle Ordovician, mostly based on biogenic phosphate oxygen isotope thermometry (e.g. Trotter et al. 2008).

Newly obtained high resolution radiochronological ages for the uppermost Katian to Hirnantian of South China (Ling et al. 2019) and for the lowermost Katian of Laurentia (Metzger et al. 2020), against well-constrained distinctive biostratigraphical horizons, can be used for anchoring floating astrochronological scales. They also impose important age constraints for the duration of Katian

and Hirnantian ages in comparison to those in published Ordovician time scales (Cooper et al. 2012; Ogg et al. 2016). Some recent studies (e.g. Lu et al. 2019, Zhong et al. 2020) illustrate the need for caution in basing cyclostratigraphical studies on condensed offshore epicratonic graptolitic shale successions without detailed sedimentological and biostratigraphical studies to identify cryptic disconformities and hiatuses.

Comparative study of the cyclostratigraphical records from high southern and subequatorial palaeolatitudes (e. g. North African and Mediterranean Gondwana versus Laurentia and Siberia) could be of outstanding importance for understanding the evolution of the Late Ordovician climate. It can provide the foundation for an astronomically calibrated time scale for the Darriwilian – Hirnantian time interval.

While the bulk, low-field, mass specific magnetic susceptibility can be successfully applied in high resolution cyclostratigraphy, it requires close support from sequence stratigraphy and biostratigraphy, preferably taken back to outcrop patterns. Otherwise it risks distortion of the calibration against geological time through lack of anchoring to well-defined biostratigraphical horizons, and unrecognised breaks, both cryptic discontinuities and larger hiatuses.

Acknowledgements

The research of M. Ghobadi Pour was completed with support from the Golestan University, Gorgan (Research Grant no 89/71/1627) and with logistical support from the National Museum of Wales, Cardiff. L. Popov acknowledges logistical support from the National Museum of Wales. We are grateful to two anonymous reviewers for constructive comments helpful in improving the manuscript.

References

Ainsaar L, Meidla T (2001) Facies and stratigraphy of the middle Caradoc mixed siliciclastic-carbonate sediments in eastern Baltoscandia. In Proceedings of the Estonian Academy of Sciences, Geology. 50:5–23.

Ainsaar L, Kaljo D, Martma T, Meidla T, Männik, P, Nõlvak, J., Tinn O (2010) Middle and Upper Ordovician carbon isotope chemostratigraphy in Baltoscandia: a correlation standard and clues to environmental history. Palaeogeography, Palaeoclimatology, Palaeoecology. 294:189–201.

Al-Husseini, M (2018) Chapter Five – Arabian Orbital Sequences, In Stratigraphy and Timescales, vol. 3 (Montenari M, Ed.). Academic Press 219–264.

Al-Husseini M. (2016a) Late Ordovician–Early Silurian orbital-forcing of glacio-eustasy. http://www.orbitalscale.net/Projects/study/AlHusseini%202016%20Orbiton %2031.pdf.

Al-Husseini M (2016b) Mid-Dapingian to Sandbian orbital-forcing of glacio-eustasy. http://www.orbitalscale.net/Projects/study/AlHusseini%202016%20Orbiton %2032.pdf.

Bergström SM, Ahlberg P, Maletz J, Lundberg F, Joachimski, MM (2018) Darriwilian (Middle Ordovician) chemostratigraphy linked to graptolite, conodont and trilobite biostratigraphy in the Fågelsång-3 drill core, Scania, Sweden. GFF 140:229–240.

Bergström SM, Bruton DL, Schmitz B, Terfelt F (2017) Local and trans-Atlantic chemostratigraphic significance of new $\delta^{13}C_{carb}$ data from the Sandbian and Katian Stages (Middle–Upper Ordovician) of the Oslo region, Norway. GFF 139:289–300.

Bergström SM, Saltzman MR, Leslie SA, Ferretti A, Young SA (2015) Trans-Atlantic application of the Baltic Middle and Upper Ordovician carbon isotope zonation. Estonian Journal of Earth Sciences. 64:8–12.

Bergström SM, Young S, Schmitz B (2010) Katian (Upper Ordovician) δ13C chemostratigraphy and sequence stratigraphy in the United States and Baltoscandia: A regional comparison. Palaeogeography, Palaeoclimatology, Palaeoecology. 296:217–234.

Boulila S, Galbrun B, Laskar J, Pälike H (2012) A~ 9 Ma cycle in Cainozoic δ13C record and long-term orbital eccentricity modulation: Is there a link?. Earth and Planetary Science Letters. 317:273–281.

Boulila S, Galbrun B, Miller KG, Pekar SF, Browning JV, Laskar J, Wright, JD (2011) On the origin of Cainozoic and Mesozoic "third-order" eustatic sequences. Earth-Science Reviews. 109:94–112.

Brett CE, Aucoin CD, Dattilo BF, Freeman RL, Hartshorn KR, McLaughlin PI, Schwalbach CE (2020) Revised sequence stratigraphy of the upper Katian Stage (Cincinnatian) strata in the Cincinnati Arch reference area: Geological and paleontological implications. Palaeogeography, Palaeoclimatology, Palaeoecology. 540:109483.

Calner M, Lehnert O, Nõlvak J (2010) Palaeokarst evidence for widespread regression and subaerial exposure in the middle Katian (Upper Ordovician) of Baltoscandia: significance for global climate. Palaeogeography, Palaeoclimatology, Palaeoecology. 296:235–247.

Chen X, Zhang Y, Li Y, Fan J, Tang P, Chen Q, Zhang Y (2012) Biostratigraphic correlation of the Ordovician black shales in Tarim Basin and its peripheral regions. Science China Earth Sciences. 55:1230–1237.

Chen X, Zhang YD, Bergström SM, Xu HG (2006) Upper Darriwilian graptolite and conodont zonation in the global stratotype section of the Darriwilian Stage (Ordovician) at Huangnitang, Changshan, Zhejiang, China. Palaeoworld. 15:150–170.

Chen X, Bergström SM, Yuandong Z, Goldman D, Qing C (2011) Upper Ordovician (Sandbian–Katian) graptolite and conodont zonation in the Yangtze region, China. Earth and Environmental Science Transactions of the Royal Society of Edinburgh. 101(for 2010):111–134.

Cherns L, Wheeley JR (2007) A pre-Hirnantian (Late Ordovician) interval of global cooling—The Boda event re-assessed. Palaeogeography, Palaeoclimatology, Palaeoecology. 251449–460.

Cherns L, Wheeley JR, Popov LE, Ghobadi Pour M, Owens RM, Hemsley AR (2013) Long-period orbital climate forcing in the early Palaeozoic?. Journal of the Geological Society. 170:707–710.

Church KD, Coe AL (2003) Processes controlling relative sea-level change and sediment supply. In The Sedimentary Record of Sea-Level Change 99–117. Cambridge University Press and the Open University, Cambridge.

Cocks LRM, Torsvik TH (2013) The dynamic evolution of the Palaeozoic geography of eastern Asia. Earth-Science Reviews. 117:40–79.

Cooper RA, Sadler PM, Hammer O, Gradstein FM (2012) The Ordovician Period. In The Geological Timescale 2012, Volume 1 (Gradstein FM, Ogg JG, Schmitz D, Ogg GM, eds). Elsevier BV, Amsterdam 489–523.

Dabard MP, Loi A, Paris F, Ghienne JF, Pistis M, Vidal M (2015) Sea-level curve for the Middle to early Late Ordovician in the Armorican Massif (western France): Icehouse third-order glacio-eustatic cycles. Palaeogeography, Palaeoclimatology, Palaeoecology. 436:96–111.

Dronov A, Holmer LE (1999) Depositional sequences in the Ordovician of Baltoscandia. Acta Universitatis Carolinae. Geologica 43:133–136.

Egenhoff S, Cassle C, Maletz J, Frisk ÅM, Ebbestad JOR, Stübner, K (2010) Sedimentology and sequence stratigraphy of a pronounced Early Ordovician sea-level fall on Baltica – the Bjørkåsholmen Formation in Norway and Sweden. Sedimentary Geology. 224:1–14.

Ellwood BB, Chrzanowski TH, Hrouda F, Long GJ, Buhl ML (1988) Siderite formation in anoxic deep-sea sediments: a synergetic bacterially controlled process with important implications in paleomagnetism. Geology. 16:980–982.

Ellwood BB, Brett CE, Tomkin JH, Macdonald WD (2013) Visual identification and quantification of Milankovitch climate cycles in outcrop: an example from the Upper Ordovician Kope Formation, Northern Kentucky. In Magnetic Methods and the Timing of Geological Process (Jovane L, Herreo-Bervara E, Hinnov LA, Housen BA, eds): 341–353. Geological Society. Special Publications 373 London.

Elrich M, Reardon D, Labor W, Martin J, Descrochers A, Pope M (2013) Orbital-scale climate change and glacioeustasy during the early Late Ordovician (pre-Hirnantian) determined from $\delta^{18}O$ values in marine apatite. Geology. 41:775–788.

Ethington RL, Clark DL (1981) Lower and Middle Ordovician Conodonts from the Ibex Area Western Millard County, Utah. Brigham Young University Geology Studies. 28:1–159.

Fang Q, Wu HC, Hinnov LA, Wang XL, Yang TS, Li HY, Zhang SH (2016) A record of astronomically forced climate change in a late Ordovician (Sandbian) deep marine sequence, Ordos Basin, North China. Sedimentary Geology 341:163–174.

Fang Q, Wu H, Wang X, Yang T, Li H, Zhang S (2019) An astronomically forced cooling event during the Middle Ordovician. Global and Planetary Change. 173:96–108.

Finney SC, Bergström SM, Chen X, Wang ZH (1999) The Pingliang section, Gansu Province, China: potential as global stratotype for the base of the *Nemagraptus gracilis* biozone and the base of the global upper Ordovician series. Acta Universitatis Carolinae, Geologica .43:73–75.

Gibbs MT, Bice KL, Barron EJ, Kump LR (2000) Glaciation in the early Paleozoic "greenhouse": the roles of paleogeography and atmospheric CO_2. In Warm climates in Earth history (Huber BT, MacLeod KG, Wing SL, eds): 386–422. Cambridge University Press, Cambridge.

Hammer Ø (2003) A 12-to 14-million year faunal diversity cycle in the Ordovician of Western Baltica. Norwegian Journal of Geology/Norsk Geologisk Forening. 83:305–314.

Haq BU, Schutter SR (2008) A chronology of Paleozoic sea-level changes. Science 322:64–68.

Harper DAT, Rasmussen CMØ, Liljeroth M, Blodgett RB, Candela Y, Jin J, Percival IG, Rong J, Villas E, Zhan RB (2013) Biodiversity, biogeography and phylogeography of Ordovician rhynchonelliform brachiopods. Geological Society, London, Memoir: 38, 127–144.

Harris WJ, Keble RA (1932) Victorian graptolite Biozones, with correlations and descriptions of species. Proceedings of the Royal Society of Victoria. 44:25–48.

Hinnov LA, Diecchio RJ (2015) Milankovitch cycles in the Juniata Formation, Late Ordovician, Central Appalachian Basin, USA. Stratigraphy. 12:287–296.

Hinnov LA, Hilgen, FJ (2012) Cyclostratigraphy and Astrochronology. In *The Geological Timescale 2012, Volume 1* (Gradstein FM, Ogg JG, Schmitz

MD, Ogg G.M, eds): 63–83. Elsevier BV, Amsterdam.

Hints L, Oraspold A, Nolvak J (2005) The Pirgu Regional Stage (Upper Ordovician) in the East Baltic: lithostratigraphy, biozonation and correlation. Proceedings of the Estonian Academy of Sciences, Geology. 54:225–259.

Holland SM, Patzkowsky ME (1997) Distal orogenic effects on peripheral bulge sedimentation; Middle and Upper Ordovician of the Nashville Dome. Journal of Sedimentary Research. 67:250–263.

Holland SM, Patzkowsky ME (1998) Sequence stratigraphy and relative sea-level history of the Middle and Upper Ordovician of the Nashville Dome, Tennessee. Journal of Sedimentary Research. 68:684–699.

Holland SM, Patzkowsky ME (1996) Sequence stratigraphy and long-term lithologic change in the Middle and Upper Ordovician of the eastern United States. In Paleozoic Sequence Stratigraphy: Views from the North American Craton (Witzke BJ, Ludvigsen GA, Day J, eds):117–130. Geological Society of America Special Paper 306.

Holm G (1881) Bidrag till kännedomen om Skandinaviens graptoliter. I. Svenska Vetenskaps-akademiens förhandlingar. 38:71–84.

Holmer LE, Ghobadi Pour M, Popov LE, Zhang Z, Zhang Z (2017) Ecology, biofacies, biogeography and systematics of micromorphic lingulate brachiopods from the Ordovician (Darriwilian–Sandbian) of south-central China. Papers in Palaeontology. 3:317–361.

Keller M, Lehnert O (2010) Ordovician paleokarst and quartz sand: Evidence of volcanically triggered extreme climates? Palaeogeography, Palaeoclimatology, Palaeoecology. 296:297–309.

Laskar J, Robutel P, Joutel F, Gastineau M, Correia ACM, Levrard B (2004) A long-term numerical solution for the insolation quantities of the Earth. Astronomy & Astrophysics. 428: 261–285.

Laskar J, Fienga A, Gastineau M, Manche H (2011) A new orbital solution for the long term motion of the Earth. Astronomy & Astrophysics 532:1–15.

Ling MX, Zhan RB, Wang GX, Wang Y, Amelin Y, Tang P, Liu JB, Jin J, Huang B, Wu RC, Xue S (2019) An extremely brief end Ordovician mass extinction linked to abrupt onset of glaciation. Solid Earth Sciences. 4:190–198.

Loi A, Ghienne,JF, Dabard MP, Paris F, Botquelen A, Christ N , Destombes J (2010) The Late Ordovician glacio-eustatic record from a high-latitude storm-dominated shelf succession: the Bou Ingarf section (Anti-Atlas, Southern Morocco). Palaeogeography, Palaeoclimatology, Palaeoecology. 296:332–358.

Long DG (2007) Tempestite frequency curves: a key to Late Ordovician and Early Silurian subsidence, sea-level change, and orbital forcing in the Anticosti foreland basin, Quebec, Canada. Canadian Journal of Earth Sciences. 44:413–431.

Matthews RK, Al-Husseini MI (2010) Orbital forcing glacio-eustasy: a sequence stratigraphic approach. GeoArabia. 15:155–167.

Matthews RK, Frohlich C (2002) Maximum flooding surfaces and sequence boundaries: comparisons between observations and orbital forcing in the Cretaceous and Jurassic (65–190 Ma). GeoArabia. 7:503–538.

Meischner T, Elicki O, Masri A, Moumani KA, Hussein MAA, Maletz J (2019) The Darriwilian Hiswah fauna of western Gondwana (Jordan): Biostratigraphy, palaeogeography and palaeoecology. Geobios. 57:53–76.

Mestre A, Heredia S (2012) Darriwilian species of Histiodella (Conodonta) in the argentine Precordillera. Alcheringa: An Australasian Journal of Palaeontology. 36:141–150.

Metzger JG, Ramezani J, Bowring SA, Fike DA (2020) New age constraints on the duration and origin of the Late Ordovician Guttenberg δ13Ccarb excursion from high-precision U-Pb geochronology of K-bentonites. GSA Bulletin **(in Press)**

Mitchell CE, Brussa ED, Astini RA (1998) A diverse Da2 fauna preserved within an altered volcanic ash fall, Eastern Precordillera, Argentina: Implications for graptolite paleoecology. In (Gutirrez-Marco JC, Rábano I, eds), Proceedings of the Sixth International Graptolite Conference of the Graptolite Working Group (IPA) and the 1998 Field Meeting of the International Subcommission on Silurian Stratigraphy (ICS-IUGS):222–223. Madrid.

Munnecke A, Zhang Y, Liu X, Cheng J (2011) Stable carbon isotope stratigraphy in the Ordovician of South China. Palaeogeography, Palaeoclimatology, Palaeoecology. 307:17–43.

Murchison RI (1839) The Silurian System, founded on geological researches in the counties of Salop, Hereford, Radnor, Montgomery, Caermarthen, Brecon, Pembroke, Monmouth, Gloucester, Worcester and Stafford: with descriptions of the Coalfields and overlying Formations. John Murray, London:768 pp.

Nielsen AT (2004) *Ordovician sea level changes: a Baltic perspective*. In The Great Ordovician Biodiversification Event (Webby BD, Paris F, Droser ML, Percival IG, eds):84–93. Columbia University Press, New York.

Ogg JG, Ogg GM, Gradstein FM (2016) A Concise Geologic Time Scale. Elsevier:240 pp.

Page A, Zalasiewicz J, Williams M, Popov L (2007) Were transgressive black shales a negative feedback modulating glacioeustasy in the Early Palaeozoic Icehouse? In Deep-Time Perspectives

on Climate Change: Marrying the Signal from Computer Models and Biological Proxies (Williams M, Haywood AM, Gregory F.J, Schmidt DN, eds):123–156. Micropalaeontological Society, Special Publications 2.

Pälike H, Frazier J, Zachos JC (2006) Extended orbitally forced palaeoclimatic records from the equatorial Atlantic Ceara Rise. Quaternary Science Reviews. 25:3138–3149.

Paris F (1990) The Ordovician chitinozoan biozones of the Northern Gondwana Domain. Review of Palaeobotany and Palynology. 66:181–209.

Paris F, Boumendjel K, Dabard MP, Ghienne JF, Loi A, Videt B , Achab A (2007) Chitinozoan-based calibration of Early-Mid Ordovician transgressive events on northern Gondwana. Acta Palaeontologica Sinica. 46:370–375.

Popov LE, Cocks RM (2017) Late Ordovician palaeogeography and the positions of the Kazakh terranes through analysis of their brachiopod faunas. Acta Geologica Polonica. 67:323–380.

Popov L, Nikitin IF, Sokiran EV (1999) The earliest atrypides and athyrididés (Brachiopoda) from the Ordovician of Kazakhstan. Palaeontology. 42:625–661.

Rasmussen CM, Nielsen AT, Harper DA (2009) Ecostratigraphical interpretation of lower Middle Ordovician East Baltic sections based on brachiopods. Geological Magazine. 146:717–731.

Saltzman MR, Young SA (2005) Long-lived glaciation in the Late Ordovician? Isotopic and sequence-stratigraphic evidence from western Laurentia. Geology. 33:109–112.

Schmitz B, Bergström SM, Xiaofeng W (2010) The middle Darriwilian (Ordovician) $\delta^{13}C$ excursion (MDICE) discovered in the Yangtze Platform succession in China: implications of its first recorded occurrences outside Baltoscandia. Journal of the Geological Society. 167:249–259.

Song SG, Niu YL, Su L, Xia XH (2013) Tectonics of the north Qilian orogen, NWChina. Gondwana Research. 23:1378–1401.

Stouge S (1984) Conodonts of the Middle Ordovician Table Head Formation, western Newfoundland. Fossils and Strata. 16:1–145.

Svensen HH, Hammer Ø, Corfu F (2015). Astronomically forced cyclicity in the Upper Ordovician and U–Pb ages of interlayered tephra, Oslo Region, Norway. Palaeogeography, Palaeoclimatology, Palaeoecology. 418:150–159.

Torsvik TH, Cocks LRM (2011) The Palaeozoic palaeogeography of central Gondwana. Geological Society, London, Special Publications, 357:137–166.

Trabucho-Alexandre J (2014) More gaps than shale: erosion of mud and its effect on preserved geochemical and palaeobiological signals. In: Smith DG, Bailey RJ, Burgess PM, Fraser AJ, eds) Strata and Time: Probing the Gaps in Our Understanding. Geological Society, London, Special Publications, 404, http://dx.doi.org/10.1144/SP404.10

Trotter JA, Williams IS, Barnes CR, Lécuyer C, Nicoll RS (2008) Did cooling oceans trigger Ordovician biodiversification? Evidence from conodont thermometry. Science. 321:550–554.

Turner BR, Armstrong HA, Wilson CR, Makhlouf IM (2012) High frequency eustatic sea-level changes during the Middle to early Late Ordovician of southern Jordan: Indirect evidence for a Darriwilian Ice Age in Gondwana. Sedimentary Geology. 251–252:34–48.

Vandenbroucke TRA, Armstrong HA, Williams M, Zalasiewicz JA , Sabbe K (2009) Ground-truthing Late Ordovician climate models using the palaeobiology of graptolites. Paleoceanography. 24:PA4202.

Vandenbroucke TRA, Armstrong HA,Williams M, Paris F, Sabbe K, Zalasiewicz JA., Nolvak J, Vermers J (2010). Epipelagic chitinozoan biotopes map a steep latitudinal temperature gradient for earliest Late Ordovician seas: implications for a cooling Late Ordovician climate. Palaeogeography, Palaeoclimatology, Palaeoecology. 294:202–219.

Videt B, Paris F, Rubino JL, Boumendjel K, Dabard MP, Loi A, Ghienne JF, Marante A, Gorini A (2010) Biostratigraphical calibration of third order Ordovician sequences on the northern Gondwana platform. Palaeogeography, Palaeoclimatology, Palaeoecology. 296:359–375.

Viira V (1974) Ordovician Conodonts of the East Baltic. Geological Institute of the Academy of Sciences of the Estonian S.S.R. Valgus, Tallinn:142 pp. (In Russian)

Wang YJ (1993) Middle Ordovician radiolarians from the Pingliang Formation of Gansu Province, China. In Radiolaria of giant and subgiant fields in Asia (Blueford J, ed.):98–114. Micropaleontology Press, New York.

Wang ZH, Bergström SM, Zhen YY, Chen X, Zhang YD (2013) On the integration of Ordovician conodont and graptolite biostratigraphy: new examples from Gansu and Inner Mongolia in China. Alcheringa: An Australasian Journal of Palaeontology. 37:510–528.

Zhang, J (1996). Lithofacies and stratigraphy of the Ordovician Guniutan Formation in its type area, China. Geological Journal. 3: 201–215.

Zhang J (1998) Conodonts from the Guniutan Formation (Llanvirnian) in Hubei and Hunan Provinces, south-central China. Stockholm Contributions in Geology. 46:1–161.

Zhang Y, Munnecke A (2016) Ordovician stable carbon isotope stratigraphy in the Tarim Basin,

NW China. Palaeogeography, Palaeoclimatology, Palaeoecology. 458:154–175.

Zhang Y, Zhan R, Zhen Y, Wang Z, Yuan , Fang X, Ma X, Zhang J (2019) Ordovician integrative stratigraphy and timescale of China. Science China Earth Sciences. 62:61–88.

Zhong Y, Wu H, Zhang Y, Zhang S, Yang T, Li H, Cao L (2018) Astronomical calibration of the Middle Ordovician of the Yangtze Block, South China. Palaeogeography, Palaeoclimatology, Palaeoecology. 505:86–99.

Zhong Y, Chen D, Fan J, Wu, H., Fang Q, Shi M (2019). Cyclostratigraphic calibration of the Upper Ordovician (Sandbian-Katian) Pagoda and Linhsiang formations in the Yichang area, South China. Acta Geologica Sinica. 93:177–180.

Zhen YY, Wang Z, Zhang YD, Bergström SM, Percival IG, Cheng J (2011) Middle to late Ordovician (Darriwilian-Sandbian) conodonts from the Dawangou section, Kalpin area of the Tarim Basin, northwestern China. Records of the Australian Museum. 63:203–266.